

# Experimental and modeling study on liquid film thickness of horizontal gas-liquid annular flow using ultrasonic method

Mi Wang <sup>a,b,\*</sup>, Yuxin Bai <sup>a,b</sup>, Jiegui Liu <sup>a,b</sup>, Dandan Zheng <sup>c</sup>, Lide Fang <sup>a,b,\*\*</sup>

<sup>a</sup> College of Quality and Technical Supervision, Hebei University, Baoding, 071000, China

<sup>b</sup> National and Local Joint Engineering Research Center for Measuring Instruments and Systems, Baoding, 071000, China

<sup>c</sup> School of Electrical and Information Engineering, Tianjin University, Tianjin, 300072, China



## ARTICLE INFO

### Keywords:

Liquid film thickness  
Ultrasonic method  
Horizontal gas-liquid annular flow  
Numerical simulation  
Prediction correlation

## ABSTRACT

In horizontal annular flow, the high gas velocity leads to the strong randomness, rapidity and complexity of the structure and dynamic characteristics of gas-liquid interfacial wave. As one of the important parameters to describe the interfacial wave, the liquid film thickness is significant to study the hydrodynamic characteristics of the gas-liquid two-phase flow. In this paper, the ultrasonic echo resonance main frequency (UERMF) method and the ultrasonic reference signal elimination (URSE) method are compared by numerical simulation method. The minimum liquid film thickness measured by these two methods are 0.3 mm and 0.01 mm, respectively. Experiments are conducted on a stainless steel test section with an inner diameter of 50.0 mm to study annular air-water flow under five different pressure conditions (from 0.1 MPa to 0.7 MPa). The experimental data is processed using the URSE method to analyze the characteristics of the liquid film under different operating conditions. In addition, based on the aforementioned experimental dataset, a comparison is made regarding the performance of existing predictive correlations. It is found that the existing correlations have certain limitations in capturing the variations of liquid film thickness in annular flow, particularly at high pressures and for different pipe diameters. Therefore, a new liquid film thickness correlation suitable for different system pressures and pipe diameters is proposed. By expanding the range of fitted data points (220 data points), the 95 % relative error of improved model is within  $\pm 25$  % error band for all available data (authors' and literature). The mean absolute percentage error (MAPE) is 11.08 %. The improved correlation has the applicability and extrapolation for different system pressure and pipe diameter conditions.

## 1. Introduction

With the development of industry, energy consumption has increased dramatically, environmental pollution is becoming more and more serious, and energy problems need to be solved urgently [1]. As a crucial link in the energy transformation process, the demands for the extraction and measurement of natural gas are continuously escalating. The vast majority of natural gas has high liquid content and high-pressure characteristics due to untreated processing after being mined [2], hence it is called wet natural gas. Wet natural gas usually presents a gas-liquid two-phase flow state during pipeline transportation. Because the annular flow has a wide range of gas and liquid flow rates, it widely exists in the field of pipeline transportation [3]. The typical feature of gas-liquid annular flow is that the gas phase is

concentrated in the center of the pipeline to form gas core, and surrounding the gas core is a liquid film that coats the inner wall of the pipe. Affected by gravity, the circumferential distribution of liquid film is not uniform, the bottom liquid film is thicker, and the top liquid film is thinner [4]. As one of the important parameters of gas-liquid two-phase flow, liquid film thickness is of great significance to study its liquid holdup, pressure drop, flow mechanism and evolution law.

The measurement methods for liquid film thickness include optical method [5], electrical method [6], nuclear radiation method [7] and ultrasonic method. In comparison to numerous measurement methods, the ultrasonic measurement method offers several advantages. It exhibits strong penetration capabilities, allowing for effective detection even in complex structures. Furthermore, ultrasonic waves can propagate over long distances, enabling measurements to be taken at considerable ranges. Additionally, this method is less reliant on the

\* Corresponding author. College of Quality and Technical Supervision, Hebei University, Baoding, 071000, China.

\*\* Corresponding author. College of Quality and Technical Supervision, Hebei University, Baoding, 071000, China.

E-mail addresses: [wangmi@hbu.edu.cn](mailto:wangmi@hbu.edu.cn) (M. Wang), [fanglide@hbu.edu.cn](mailto:fanglide@hbu.edu.cn) (L. Fang).

<b>Nomenclature</b>	
<i>English symbols</i>	
$b(t)$	The reflected signal of the plexiglass-water interface
$b(n)$	The discrete time series of $b(t)$
$c$	The sound velocity in water
$D$	Pipe diameter
$d(t)$	The reflected signal of water-air interface
$d(n)$	Discrete time series of reflection signals at the water-air interface
$d_{32}$	Sauter average diameter
$E$	Entrainment rate
$E_m$	Maximum entrainment rate
$e_f$	Error of UERMF method
$e_x$	Error of URSE method
$F$	A parameter proposed by Henstock
$f_m$	The semi-resonant frequencies
$f_s$	Sampling frequency
$Fr$	Froude number
$G$	Mass flux
$g$	Gravity acceleration
$h$	The liquid film thickness
$\bar{h}$	Average liquid film thickness
$h_{of}$	The simulation results of the UERMF method
$h_{ox}$	The simulation results of the URSE method
$h^*$	Dimensionless form of $h$
$L$	The displacement parameter
$m_{lf_c}$	Critical liquid membrane mass flow
$m_l$	Liquid mass flow
$m$	The semi-resonant orders
$N$	Data length
$n$	$n$ -th data point
$p$	Pressure
$R_d(\sigma)$	Cross-correlation function
$Re$	Reynolds number
$s$	Standard deviation
$u$	Velocity
$\nu$	Kinematic viscosity
$x$	Dryness
<i>Greek symbols</i>	
$\sigma$	Liquid surface tension
$\rho$	Density
$\mu$	Dynamic viscosity
$\tau$	Shear force
<i>Subscripts</i>	
$g$	Gas phase
$ref$	Reference
$sg$	Gas superficial phase
$sl$	Liquid superficial phase
$lf$	Liquid film
$l$	Liquid phase

specific characteristics of the target structure and is minimally affected by the testing environment [8]. Consequently, the ultrasonic measurement method finds extensive application in various industrial measurement scenarios. Ultrasonic pulse echo method is the earliest and most widely used ultrasonic method for measuring liquid film thickness [9]. For the thick liquid film (above the order of mm), this method can determine liquid film thickness by measuring the time difference between the reflected pulse waves from both sides. However, when the liquid film becomes thinner and thinner, these two reflected waves will be superimposed in the time domain [10], making it challenging to obtain the time difference. Therefore, the ultrasonic pulse echo method cannot calculate the thinner liquid film.

In view of the limitations of the traditional ultrasonic pulse echo method, scholars proposed the film resonance method to realize the measurement of thinner oil film [11]. However, in the case of gas-liquid two-phase flow with complex flow conditions, the presence of liquid film fluctuations and multiple echoes can introduce numerous reflections into the measurement results. This can pose challenges in accurately determining the resonant frequency and number of resonances [12]. Therefore, our research group proposed the ultrasonic echo resonance main frequency (UERMF) method [13] to solve the problem that the resonance frequency and resonance number are difficult to determine due to multiple echoes, noise interference and liquid film fluctuation. However, owing to the limitation of the center frequency and bandwidth of ultrasonic transducer, the minimum liquid film thickness is 0.3 mm for a 5 MHz ultrasonic transducer. In the actual measurement, the liquid film on the top and both sides of the horizontal tube are very thin, and most of the film thickness is below 0.3 mm. Furthermore, the measurement accuracy of the ultrasonic transducer is influenced by factors such as the manufacturing process and technical capabilities, which limits the effectiveness of the UERMF method for measuring thinner liquid film.

For purpose of measuring thinner liquid film, researchers have proposed the ultrasonic reference signal elimination (URSE) method based on the traditional ultrasonic pulse echo method, which further expands

the range of liquid film thickness by ultrasonic method. In 2014, Aoyama et al. [14] developed a prototype liquid film sensor for high-temperature steam-water experiments to measure the liquid film thickness. The minimum liquid film thickness obtained by URSE method could reach 0.084 mm. In 2017, Praher et al. [15] proposed an algorithm for reconstructing this superimposed signal in the time domain. By comparing simulated and measured signals, the time difference of the ultrasonic pulse in a layer could be estimated and the layer thickness could then be calculated. In laboratory measurements, the author validated successfully (maximum relative error 4.9 %) this algorithm for layer thicknesses ranging from 0.03 mm to 0.2 mm. In 2019, Al-Aufi et al. [16] used the URSE method to measure the liquid film thickness under static conditions. The minimum liquid film thickness could reach 0.1 mm, and the maximum measurement error is 2 %. Then this studied method was tested on downward and upward vertical flow experimental rigs with pipe diameters of 34.5 mm and 127 mm respectively. For the liquid film with thickness from 0.5 mm to 2.5 mm, the experimental results demonstrated that ultrasonic method and conductivity probe method were in good agreement, and the relative error was less than 5 %. In summary, the URSE method further expands the lower limit of liquid film thickness measurement. However, this method is mainly used in static liquid film thickness. In addition, existing researches focus on the dynamic liquid film thickness measurement in vertical gas-liquid two-phase flow, but this may not fully reflect the applicability of the URSE method. Therefore, the measurement range and application of the URSE method in horizontal gas-liquid two-phase flow is studied in this paper, so that it can better realize the measurement for thin liquid film in horizontal gas-liquid two-phase flow.

Compared with single-phase flow, the flow mechanism of two-phase flow is more complex and the experimental measurement is more difficult. The researches show that the gas-liquid two-phase flow is important in industrial construction and it affects the design and operation reliability and safety of industrial equipment. The liquid film thickness is closely related to the flow states, medium conditions and pipeline situations. So, it is of great significance to establish a reliable

and accurate liquid film thickness correlation for the study of two-phase flow. In 1976, Henstock et al. [17] established a correlation for the circumferential liquid film thickness in vertical and horizontal tube by correlating the gas-phase friction coefficient with the annular liquid film thickness. However, data available for horizontal flows were not sufficient to establish an accurate relation for the liquid film thickness, the fitting effect of the horizontal prediction correlation was not as good as for the vertical correlation. In 1977, Tatterson et al. [18] pointed out that the influence of gravity must be taken into account in Henstock empirical correlation. Consequently, gravity factor was introduced into Henstock model, which greatly improved the accuracy of liquid film thickness prediction. In 1978, Hori et al. [19] conducted an experiment to collect the information on main parameters characterizing the air-water interface. Based on their experiment, a new correlation between the interfacial friction factor and the liquid film thickness was established. In the subsequent study, it was applied to air-glycerol aqueous solution annular flow, which have good prediction results. Fukano et al. [19] found that the correlation by Hori et al. gave larger prediction values especially where the liquid film thickness became small. In 1998, Fukano et al. [19] investigated the effects of liquid viscosity on the film thickness and proposed their correlations. But it was only applicable to the pipeline of 26 mm diameter at atmospheric pressure. In 2009, Schubring et al. [20] pointed out that measurements of liquid base film thickness distribution had obtained for horizontal annular two-phase (air-water) flow conditions in 8.8 mm, 15.1 mm, and 26.3 mm ID tubes. An iterative critical friction factor model was used to model circumferentially-averaged base film thickness; an explicit, empirical correlation was also provided. Due to the influence of gas flow, the relation might have prediction deviations beyond the specific range of conditions. Additional experimental data should be brought into the fitting to achieve better prediction results. In 2014, Berna et al. [21] analyzed the applicability of existing prediction correlations and fitted a comprehensive prediction correlation based on a large number of experimental data under different working conditions. After research and comparison, it was found that the correlation was not accurate in predicting liquid film thickness in high pressure system. In 2017, Setyawan et al. [22] proposed a circumferential liquid film prediction correlation that could predict liquid film thickness in 26 mm pipes, but the correlation was not suitable for other diameter pipes and did not have good universality. Although scholars have done a lot of work, the correlation of liquid film thickness under different pressures and different pipe diameters were rarely studied by scholars. Therefore, the pressure, pipe diameter and entrainment are improved based on the existing liquid film thickness correlation in this paper, so that the new correlation can better realize the prediction of liquid film thickness.

In this paper, the URSE method and UERMF method are compared by

numerical simulation, the ultrasonic measurement system is designed and the circumferential liquid film thickness data is measured at 0.1–0.7 MPa pressure. The URSE method selected to process the experimental data and analyzed the variation law of liquid film thickness. Furthermore, the asymmetry characteristic parameters with gas-liquid ratio and system pressure are also studied. By analyzing and modeling the results of liquid film thickness, the correlations of Berna, Pan, and Hurlburt are combined. So that the new correlation can adapt to the prediction of liquid film in pipelines with different pressures and diameters.

## 2. Measurement principle of ultrasonic reference signal elimination method

The ultrasonic pulse echo method measures the liquid film thickness by calculating the ultrasonic signal echo time difference, as shown in Fig. 1. Although this method is mature and simple, the ultrasonic echo signal will be superimposed for the thin liquid film below 1 mm, so the traditional ultrasonic pulse echo method is no longer applicable.

Scholars put forward the film resonance method to measure the micron oil film in mechanical bearing. In real bearing, three-layer structure is steel-oil-steel, while for the plexiglass-water-air three-layer medium used in gas-liquid annular flow, the spectrum of reflection coefficient will be interfered by multiple echoes and noise, resulting in the unsatisfactory measurement effect of the film resonance method. So, researchers improved this method and proposed the UERMF method to solve above problem [13].

### 2.1. Ultrasonic echo resonance main frequency method

The UERMF method [13] is based on the film resonance method to perform a second FFT to obtain the main frequency  $\Delta f$  which can be used to obtain the liquid film thickness  $h$ . In the plexiglass-water-air three-layer medium, the reflection coefficient reaches the minimum value at the half-resonant frequency, so the liquid film thickness in middle layer is:

$$h = \frac{c \cdot m}{4f_m} \quad (m = 1, 3, 5, \dots) \quad (1)$$

Substituting  $\Delta f = f_{m+2} - f_m$  into Eq. (1), and  $h$  can be calculated by Eq. (2) as follows:

$$h = \frac{c}{2 \cdot \Delta f} \quad (2)$$

where  $f_m$  and  $m$  are the semi-resonant frequencies and orders respectively,  $c$  is the sound velocity in water.

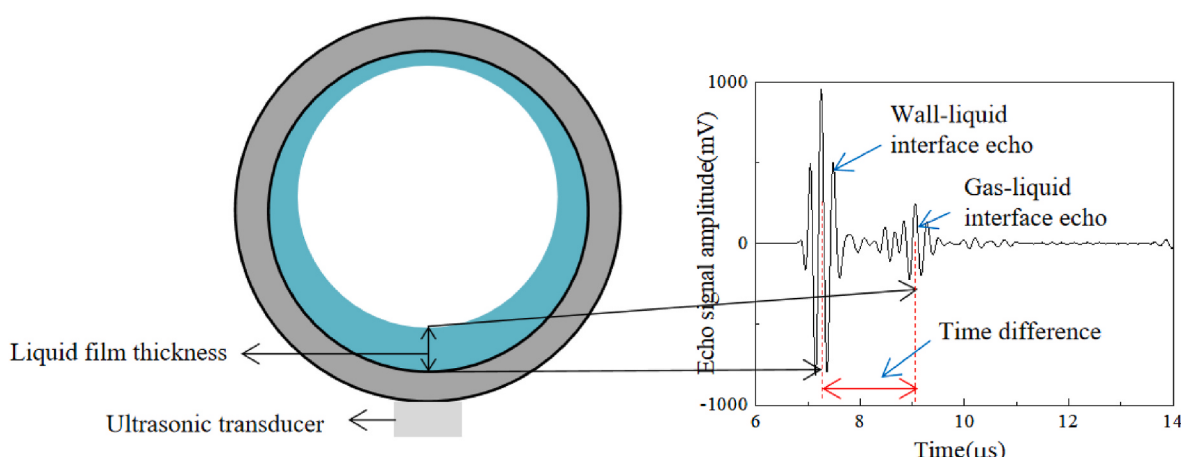


Fig. 1. Principle diagram of pulse echo reflection method.

## 2.2. Ultrasonic reference signal elimination method

The basic principle of URSE method [25] is shown in Fig. 2.  $s(t)$  represents the reflected signal of the plexiglass-water-air interface, including the reflected signal of the plexiglass-water interface (the reference signal  $b(t)$ ) and the reflected signal of the water-air interface. The reflected signals of these two interfaces are visibly superimposed, making it challenging to differentiate between the two signals. The reflected signal from the water-air interface is commonly referred to as the differential signal, denoted as  $d(t)$ , which is obtained by subtracting  $b(t)$  from  $s(t)$ . The time difference  $\Delta t$  between  $b(t)$  and  $d(t)$  is the propagation time of the sound wave in the water, which is calculated by cross-correlation method as shown in Eq. (3).

$$R_d(L) = \sum_{n=1}^N d(n)b(n-L) \quad (3)$$

where  $R_d(L)$  is the cross-correlation function,  $N$  is the data length,  $d(n)$  and  $b(n)$  are the discrete time series of  $d(t)$  and  $b(t)$ , and  $L$  is the displacement parameter. When  $R_d(L)$  reaches its maximum value, the correlation between  $d(n)$  and  $b(n)$  is highest. At this point, we designate the displacement parameter  $L$  as  $L_0$ . The time difference  $\Delta t$  can be calculated by displacement  $L_0$  and sampling frequency  $f_s$ , as shown in Eq. (4).

$$\Delta t = \frac{L_0}{f_s} \quad (4)$$

The liquid film thickness  $h$  can be calculated by Eq. (5).

$$h = \frac{c \cdot \Delta t}{2} \quad (5)$$

## 2.3. Simulation results and analysis

Due to the limitations in experimental methods for constructing thinner liquid film thickness, this paper utilizes numerical simulation to compare the performance of the UERMF method and URSE method in measuring thinner liquid film thickness. To achieve this, an electrical circuit module is incorporated into the acoustic-piezoelectric module,

forming an integrated simulation model that accounts for electrical circuit, electrostatics, solid mechanics, and pressure acoustics multi-physics coupling. This simulation model can produce direct and converse piezoelectric effects, so as to realize the function of transmitting and receiving signals by ultrasonic transducers. The simulation pipeline is made of plexiglass with an inner diameter of 50 mm. The center frequency of the ultrasonic transducer is 5 MHz, the piezoelectric film is 0.4 mm PZT-5H material, and the backing material is 2 mm aluminum. The simulation diagram of sound wave propagation process is shown in Fig. 3.

The simulation results are shown in Table 1. The theoretical liquid film thickness  $h_0$  is 0.1 mm, 0.2 mm, 0.8 mm, 1 mm, 3 mm.  $h_{0f}$  and  $h_{0x}$  are the simulation results of the UERMF method and the URSE method,  $e_f$  and  $e_x$  are the relative errors between these two methods and simulation values.

It can be seen that when the liquid film is thick, the errors  $e_f$  and  $e_x$  are relatively small, and both methods can obtain accurate liquid film thickness within a certain range. However, at liquid film thicknesses of 0.1 mm and 0.2 mm, the error  $e_f$  becomes significantly larger, indicating that the UERMF method lacks accuracy for film thicknesses below 0.3 mm. In contrast, the error  $e_x$  is only 1.7 % and 1.3 % when the liquid film thickness is 0.1 mm and 0.2 mm. The URSE method makes up for the deficiency of the UERMF method in handling the extremely thin liquid film, and expands the lower limit of the ultrasonic method for liquid film thickness measurement.

Two typical simulation results are selected to analyze the applicability of these two methods, also to explain the advantages of the URSE method. Fig. 4 presents the signal processing of the UERMF method and the URSE method for the liquid film thickness of  $h_0 = 3$  mm and the simulation results of two methods are  $h_{0f} = 2.959$  mm and  $h_{0x} = 2.988$  mm. When the liquid film is thick, the UERMF method exhibits a more prominent resonance frequency, and the two echo signals of the URSE method do not significantly overlap. Both methods can easily calculate the accurate liquid film thickness.

As shown in Fig. 5, the simulation results for 0.1 mm liquid film are  $h_{0f} = 0.209$  mm and  $h_{0x} = 0.102$  mm, respectively. Due to the thin liquid film below 0.3 mm, there is no resonance frequency in the spectral diagram of reflection coefficient, that is, the main frequency does not exist,

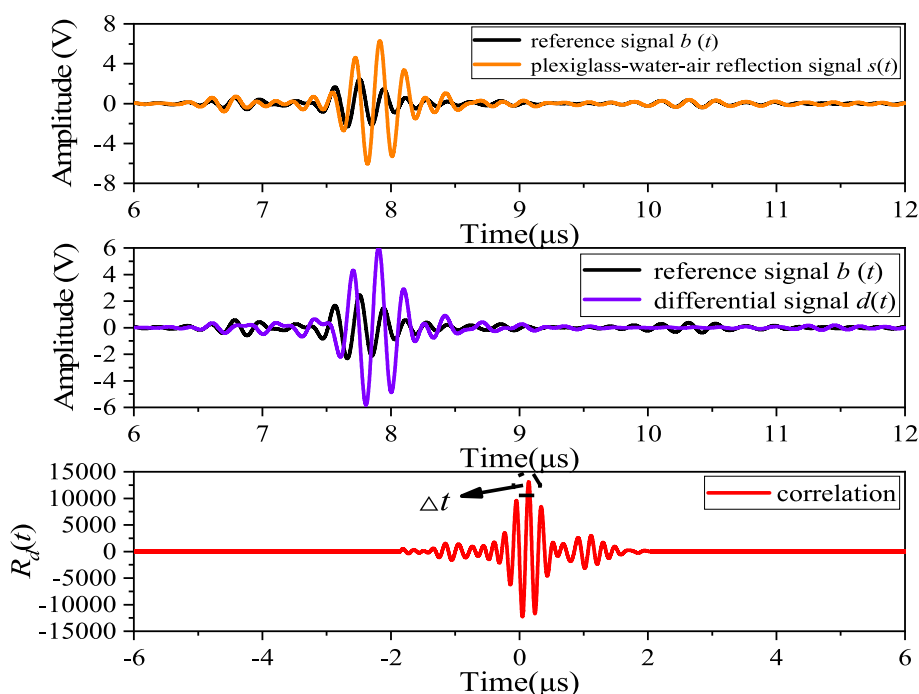


Fig. 2. The schematic diagram of URSE method.

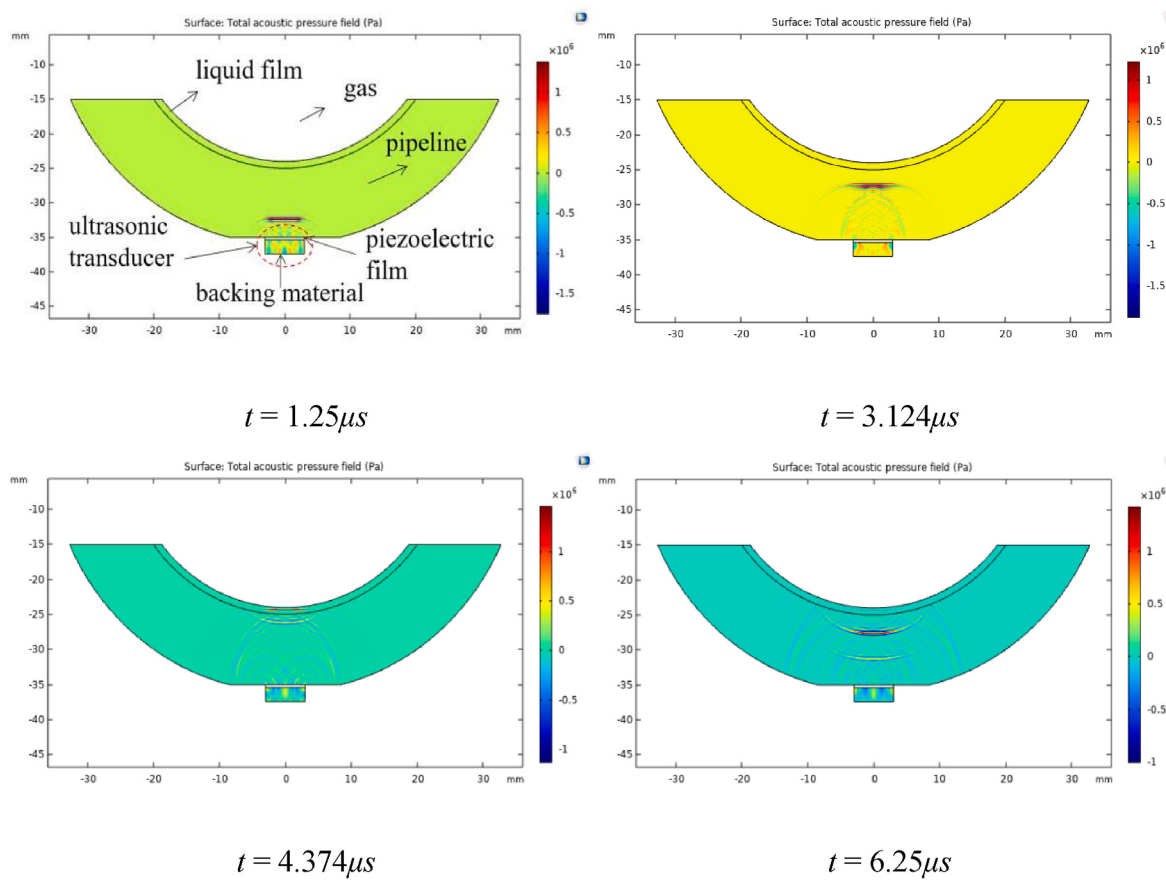


Fig. 3. The simulation diagram of sound wave propagation process.

**Table 1**  
Simulation results of liquid film thickness.

$h_0$ (mm)	$h_{0f}$ (mm)	$h_{0x}$ (mm)	$e_f$ (%)	$e_x$ (%)
0.1	0.209	0.102	108.700	1.700
0.2	0.644	0.203	221.900	1.300
0.8	0.793	0.800	-0.838	-0.250
1	0.987	1.000	-1.280	-0.030
3	2.959	2.988	-1.383	-0.397

so the UERMF method cannot accurately obtain the liquid film thickness. However, due to the fact that the URSE method is through the difference between the echo signal and the reference signal, it can distinguish the reflected signal at different interfaces very well, it is not affected by multiple echoes and can accurately obtain the liquid film thickness. The URSE method has its unique advantages, and also has high accuracy for extremely thin film. Thus, the URSE method can be applied to measure both thinner and thicker liquid film, which is used in the subsequent measurement for circumferential liquid film thickness. Additionally, the measurement accuracy of this URSE method is related to the sampling frequency. In this paper, a sampling frequency of 80 MHz is utilized, allowing for a minimum liquid film thickness of 0.01 mm.

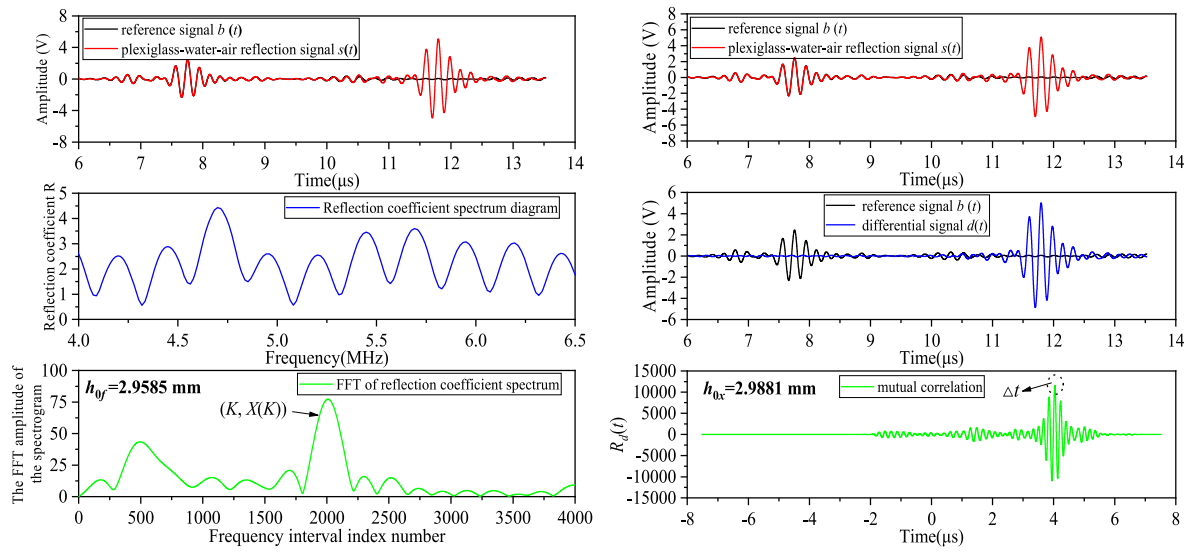
### 3. Experimental device and experimental results

#### 3.1. Experimental device

The experiments are conducted using the double closed-loop wet gas experimental device at Tianjin University, as depicted in Fig. 6. The device includes gas phase loop and liquid phase loop. The test section

inner diameter is 50 mm. The gas standard meter utilizes a turbine flow meter and achieves a measurement accuracy of 1.0 % within the range of 10–400 m<sup>3</sup>/h. The liquid standard meter is an electromagnetic flow meter which has a measurement accuracy of 0.35 % for the range of 0.05–8 m<sup>3</sup>/h. In the gas phase loop, the external air is compressed to attain the desired experimental pressure. The compressed air is then entered into the gas phase loop through the piston fan. In the liquid phase loop, the water enters the mixer through the liquid pump. The mixer facilitates the mixing of air and water, resulting in a gas-liquid two-phase flow. The gas-liquid two-phase flow is separated into air and water through the separator, and then the two-phase fluids return to their own loop.

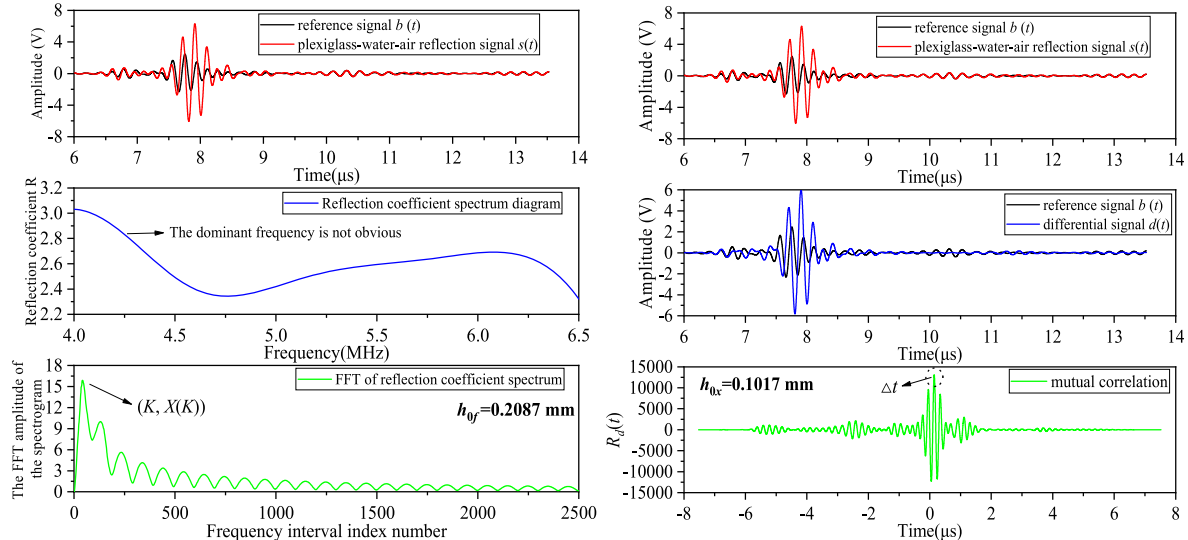
The horizontal test section is mainly composed of a multi-channel synchronous ultrasonic measurement system, including self-developed transceiver circuit, ultrasonic sensor and data acquisition system, as shown in Fig. 7. The self-developed transceiver circuit mainly contains power module, FPGA (Field-Programmable Gate Array) module, transmitting module, transceiver isolation module and receiving module. The ultrasonic sensor is installed on a plexiglass tube with the diameter of 50 mm, and the signal transmission and reception realize by means of self-transceive. Generally, it is considered that the liquid film distribution in horizontal tube is radial symmetrical, so seven ultrasonic transducers are successively installed on one side of the pipe from the bottom (0°) to the top (180°). The self-developed ultrasonic transceiver circuit generates electrical signals at a pulse repetition frequency of 100 Hz to stimulate the ultrasonic transducer. The data acquisition system, with an 80 MHz sampling frequency, records and stores the measured liquid film thickness data obtained from this measurement system. Lastly, the computer saves and processes the collected 60-s data.



(a) UERMF method

(b) URSE method

Fig. 4. The signal processing of two methods (3 mm liquid film thickness).



(a) UERMF method

(b) URSE method

Fig. 5. The signal processing of two methods (0.1 mm liquid film thickness).

### 3.2. Circumferential liquid film fluctuation characteristics

In annular flow experiment, the gas superficial velocity  $u_{sg}$  is 20, 25, 30 m/s, the liquid superficial velocity  $u_{sl}$  is 0.015, 0.035, 0.06, 0.1, 0.2, 0.3, 0.4, 0.5, 0.6 m/s, and the pressure  $p$  is 0.1, 0.2, 0.3, 0.5, 0.7 MPa. Through measuring above working conditions, the liquid film thickness data are successfully obtained. As shown in Fig. 8, some the experimental measurement results of liquid film fluctuation with time at different circumferential positions are given under the system pressure of 0.3 MPa, gas superficial velocity of 30 m/s and liquid superficial velocity of 0.035 m/s, 0.06 m/s, 0.1 m/s.

In general, the liquid film thickness and fluctuation intensity in the lower part of the pipeline are greater than those in the upper part of the pipeline, and gradually decrease from the bottom to the top of the

pipeline. In the gas-liquid two-phase annular flow, the circumferential liquid film is thicker at lower  $u_{sg}$  and higher  $u_{sl}$ . Furthermore, it is observed that as the system pressure ( $p$ ) increased, the circumferential liquid film become progressively thinner.

Besides, the time-averaged liquid film thickness  $h$  and standard deviation  $s$  are used to describe the fluctuation of the liquid film at different circumferential positions under different working conditions as follows. Fig. 9 presents the variation of the liquid film at different circumferential positions with the gas superficial velocity  $u_{sg}$  under  $p = 0.3$  MPa and  $u_{sl} = 0.035$  m/s.

It can be seen from Fig. 9 that the liquid film is becoming increasingly stable from the bottom to the top. As  $u_{sg}$  increases, the liquid film thickness of the lower part of the pipeline ( $0^\circ$ – $90^\circ$ ) gradually decreases, and the liquid film gradually tends to be stable. At the upper half of the

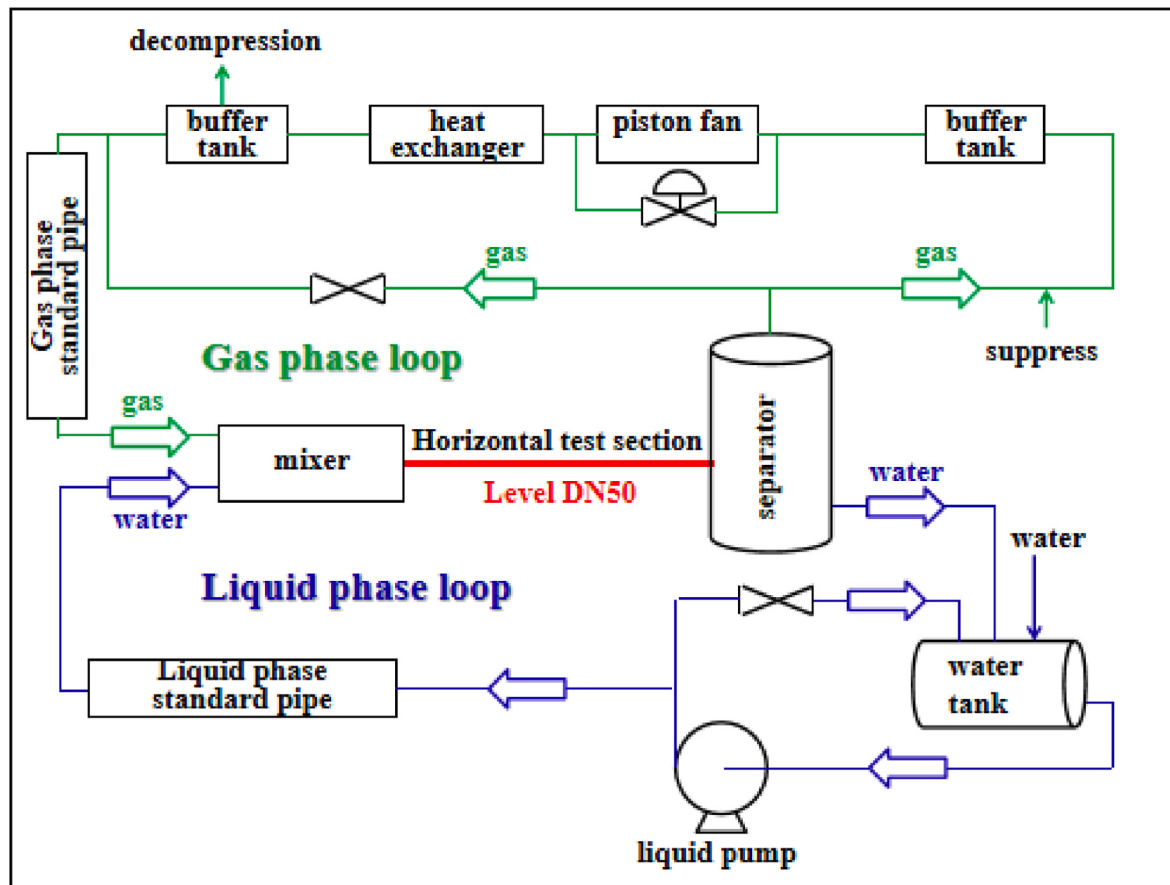


Fig. 6. The schematic diagram of wet gas device.

pipe ( $120^\circ$ – $180^\circ$ ), with the increase of  $u_{sg}$ , the liquid film thickness increases gradually and the fluctuation of the liquid film is more intense.

Under specific conditions of system pressure ( $p$ ) and liquid superficial velocity ( $u_{sl}$ ), it is observed that the intensity of disturbance wave fluctuations increases with higher gas superficial velocity ( $u_{sg}$ ). Notably, the bottom liquid film tends to exhibit an upward transport trend driven by disturbance waves and liquid entrainment. It will cause the liquid film thickness in the lower half of the pipeline to become thinner and the liquid film to become more stable, while the thickness of the liquid film in the upper half of the pipeline will become thicker and the fluctuations will become more severe. While the liquid film in the upper half of the pipeline shows an opposite changing trend. The transition region of this change trend is generally at  $90^\circ$ .

Fig. 10 presents the variation of the liquid film at different circumferential positions with the liquid superficial velocity  $u_{sl}$  under  $p = 0.3$  MPa and  $u_{sg} = 30$  m/s. When  $u_{sl}$  is constant, the standard deviations of the lower part of the pipeline ( $0^\circ$ – $90^\circ$ ) is much larger than that of the upper part of the pipeline ( $120^\circ$ – $180^\circ$ ), and the liquid film at the bottom of the pipeline fluctuates more violently. As  $u_{sl}$  increases, the fluctuation becomes more intense. From the bottom to the top of the pipe, the standard deviation  $s$  shows a decreasing trend, the liquid film is more stable, indicating that the disturbance wave in the lower half of the circumferential position cannot completely reach the top. Especially at  $120^\circ$  position, the standard deviation shows a rapid growth trend, and the disturbance wave has obviously reached this position, showing a trend of transition to the top.

The shear stress between the gas-liquid interface is enhanced with the increase of  $u_{sl}$ . Driven by the strong force, the disturbance wave reaches the top of the pipeline, and the liquid entrainment is enhanced accordingly, resulting in the increase of the liquid film thickness in the upper part of the pipeline and the more severe fluctuation [22], while

the thickness and fluctuation of the liquid film in the lower part will increase accordingly due to the increase of the liquid phase.

As shown in Fig. 11, at the same gas-liquid superficial velocity, as the pressure in the pipeline increases, the thickness and fluctuation of the liquid film in the lower half of the pipeline gradually decrease, while the liquid film in the upper half of the pipeline shows an opposite changing trend. There is a transition zone at  $90^\circ$  and  $120^\circ$ , which is very similar to the effect of  $u_{sg}$  on the circumferential liquid film.

The increase in system pressure has two main effects on the annular flow dynamics. Firstly, it leads to more stable liquid film and a decrease in liquid film thickness in the lower part of the pipeline. Secondly, it increases the shear stress at the gas-liquid interface. The increase of system pressure is mainly reflected in two aspects: stable liquid film and driving disturbance wave climbing from the bottom of the pipeline to the surrounding. The disturbance wave at the gas-liquid interface climbs to the top of the pipeline under the action of shear force, and the droplets are entrained by the disturbance wave. The entrained droplets also reach the top of the pipeline, increasing the liquid film thickness at the top, making the liquid film fluctuation more obvious. Therefore, under different working conditions, the influence of system pressure on the liquid film thickness and fluctuation trend at different positions of the pipeline is different, which should be considered according to the specific situation.

### 3.3. Asymmetry analysis of circumferential liquid film

The circumferential liquid film asymmetry is an important index to describe the liquid film thickness in horizontal tube. Two asymmetry indexes  $\bar{h}/h_0$  and  $h_{180}/h_0$  are given to analyze the asymmetry of liquid film under different working conditions, which are the ratio of the average liquid film thickness  $\bar{h}$  to the bottom thickness  $h_0$  and the ratio of

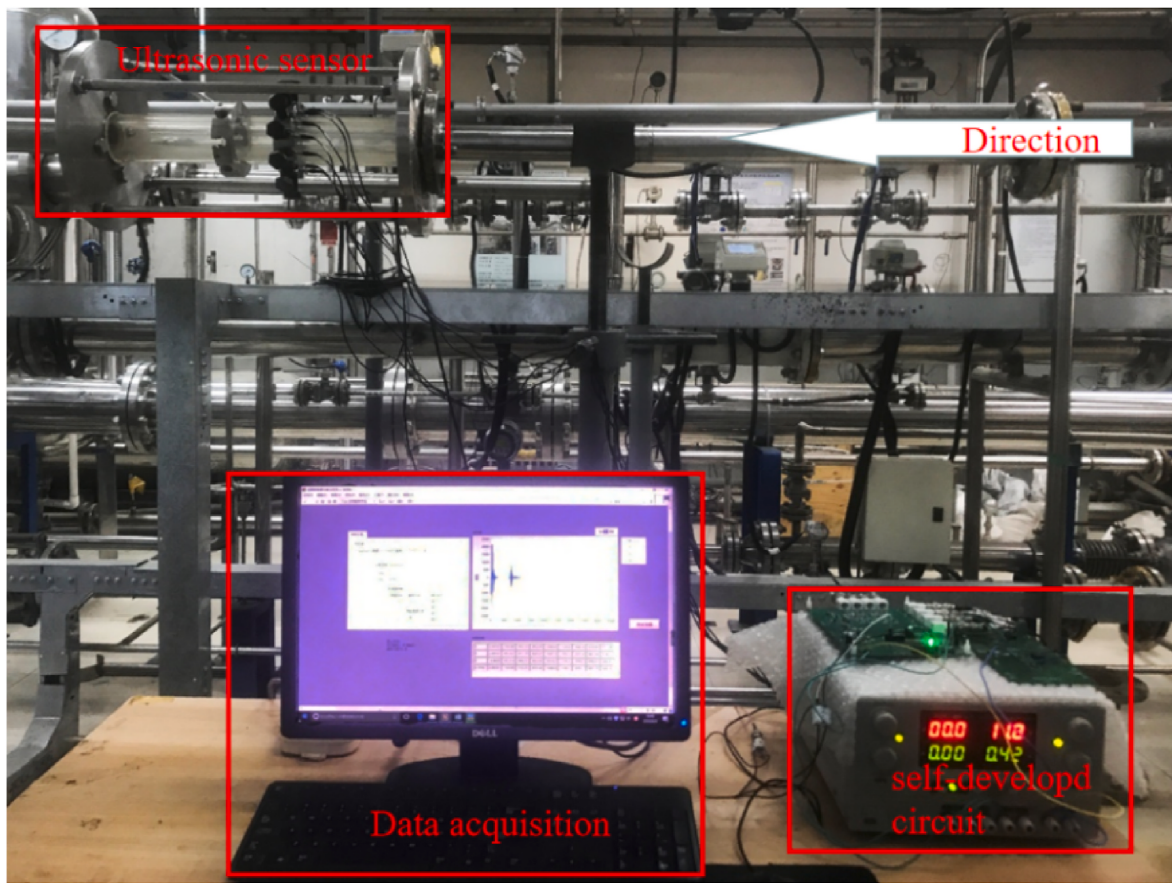


Fig. 7. Multi-channel synchronous ultrasonic measurement system.

the top liquid film thickness  $h_{180}$  to the bottom liquid film thickness  $h_0$ . The smaller the two indexes are, the more serious the asymmetry of the liquid film, and the larger the two indexes are, the better the symmetry. When these two indexes are both equal to 1, it indicates that the thickness of the liquid film thickness at different circumferential positions is equal, and the symmetry is the best.

The asymmetry of circumferential liquid film depends on the flow conditions of the gas-liquid two-phase flow. It can be seen from Table 2 that under certain conditions of  $u_{sl}$  and  $p$ ,  $\bar{h}/h_0$  and  $h_{180}/h_0$  will increase significantly with the increase of  $u_{sg}$ . It indicates that increasing the  $u_{sg}$ , the asymmetry of circumferential liquid film will decrease, and the circumferential distribution of liquid film tends to be more uniform. Usually, when the  $u_{sg}$  is low, the liquid phase does not have enough ability to reach the top of the pipe due to the influence of gravity and the pipe wall friction, so that the liquid phase mostly flows at the bottom of the pipe. However, with the increase of the  $u_{sg}$ , the force between gas phase and liquid phase becomes stronger, and the fluctuation of disturbance wave becomes more intense. Under the influence of droplet entrainment-deposition and secondary flow mechanism, the effect of the bottom liquid film spreading to the circumferential direction is strengthened, so the top liquid film thickness gradually increases and the asymmetry of the circumferential liquid film decreases.

With the increase of  $u_{sl}$ , both  $\bar{h}/h_0$  and  $h_{180}/h_0$  show a decreasing trend. It indicates that with the increase of  $u_{sl}$ , although the liquid film thickness in the upper and lower parts of the pipeline will increase, the degree of increase in the upper part is much smaller than that in the lower part, resulting in a more pronounced asymmetry in the circumferential liquid film. In general, the effect of  $u_{sg}$  on the asymmetry of circumferential liquid film is more significant than that of  $u_{sl}$ .

Furthermore, it is evident that increasing the system pressure ( $p$ ) leads to a reduction in the asymmetry of the circumferential liquid film,

resulting in a more even distribution of the liquid film across different positions. This is because as the pressure increases, the suction effect of the disturbance wave becomes stronger, and the shear force at the gas-liquid interface increases, thereby making the liquid film overcome gravity and transport to the top. From the analysis in Section 3.2 above, it can be seen that increasing the system pressure can also stabilize the liquid film of different positions, thus weakening the asymmetry of the circumferential liquid film. The system pressure and gas superficial velocity have similar effects on the asymmetry of circumferential liquid film.

#### 4. A new correlation for predicting circumferential average liquid film thickness

##### 4.1. Comparison and analysis of the existing liquid film thickness correlations

The accurate prediction of liquid film thickness has always been a problem that many scholars have been striving to explore. So far, many scholars have proposed many liquid film thickness correlations under different working conditions.

In 1976, Henstock et al. [17] correlated film thickness with limited horizontal experimental data and found the best fit correlation is shown in Eq. (6)

$$\frac{h}{D} = \frac{6.59F}{(1 + 850F)^{0.5}} \quad (6)$$

The definition of parameter  $F$  is as follows.

$$F = \frac{1}{\sqrt{2}Re_g^{0.4}} \frac{Re_l^{0.5}}{Re_g^{0.9}} \frac{\mu_l}{\mu_g} \frac{\rho_g^{0.5}}{\rho_l^{0.5}} \quad (7)$$

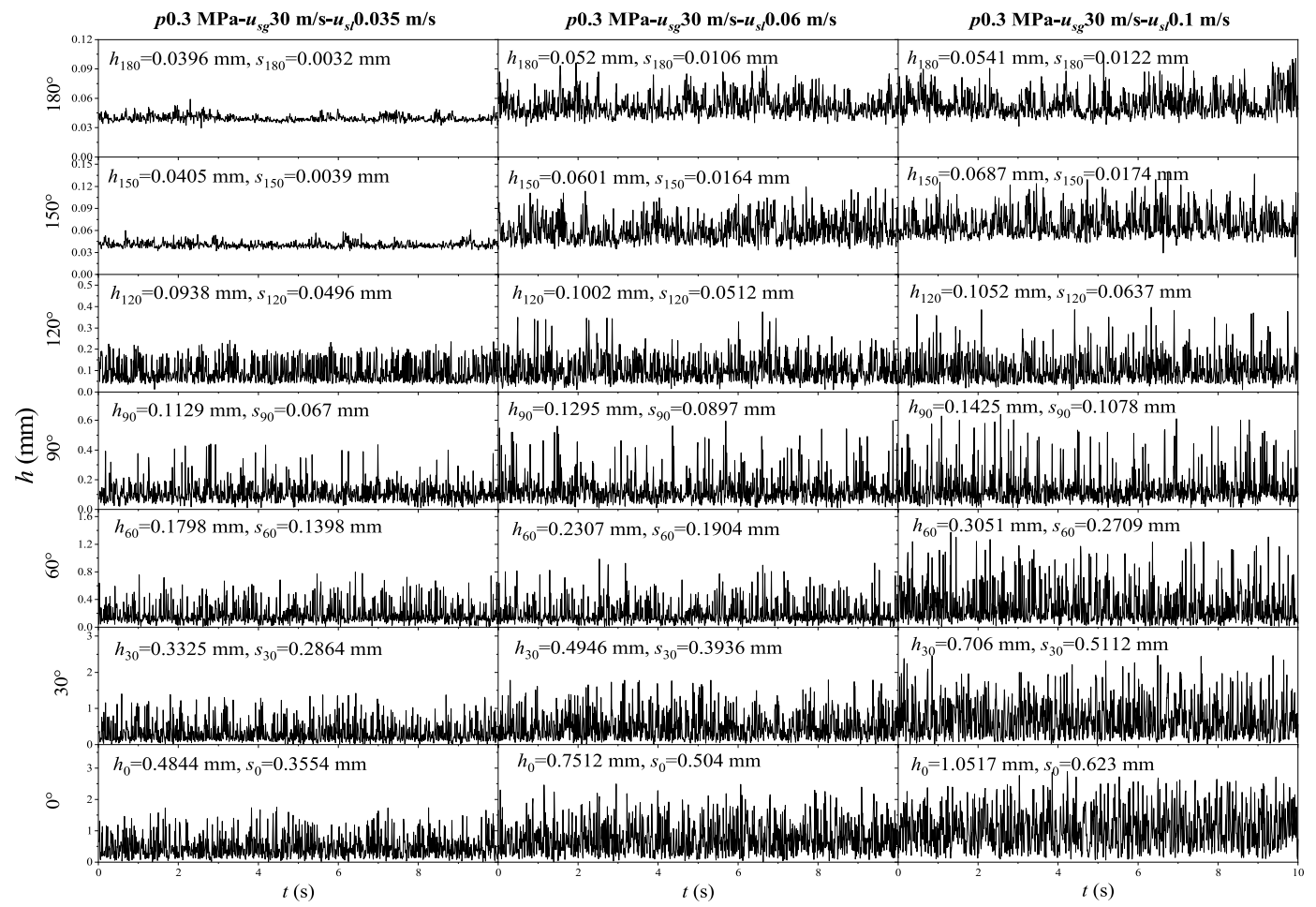


Fig. 8. The fluctuation of liquid film with time at different positions in the circumferential direction.

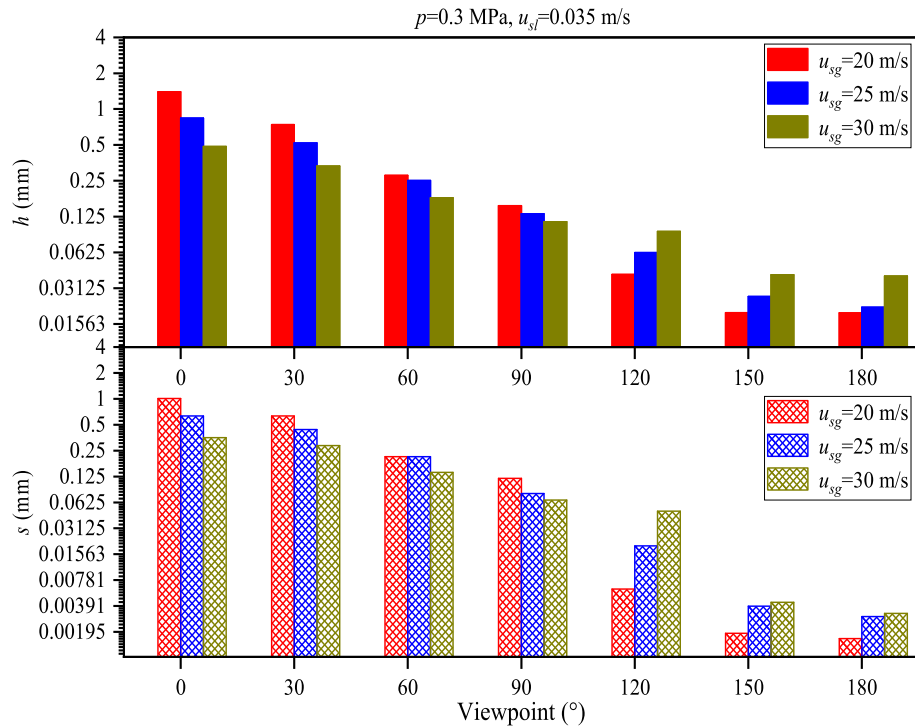
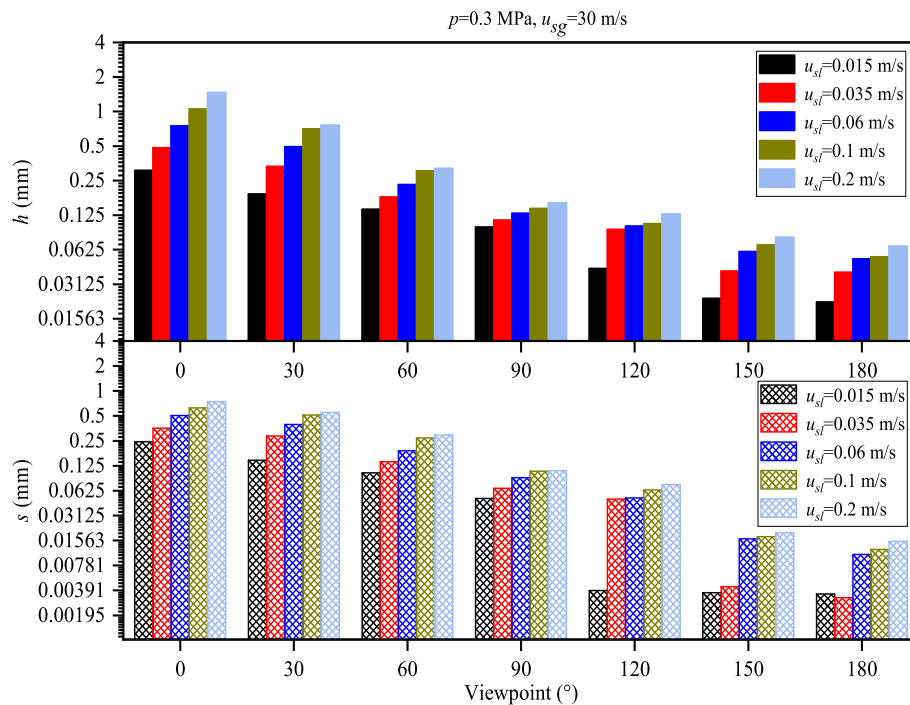
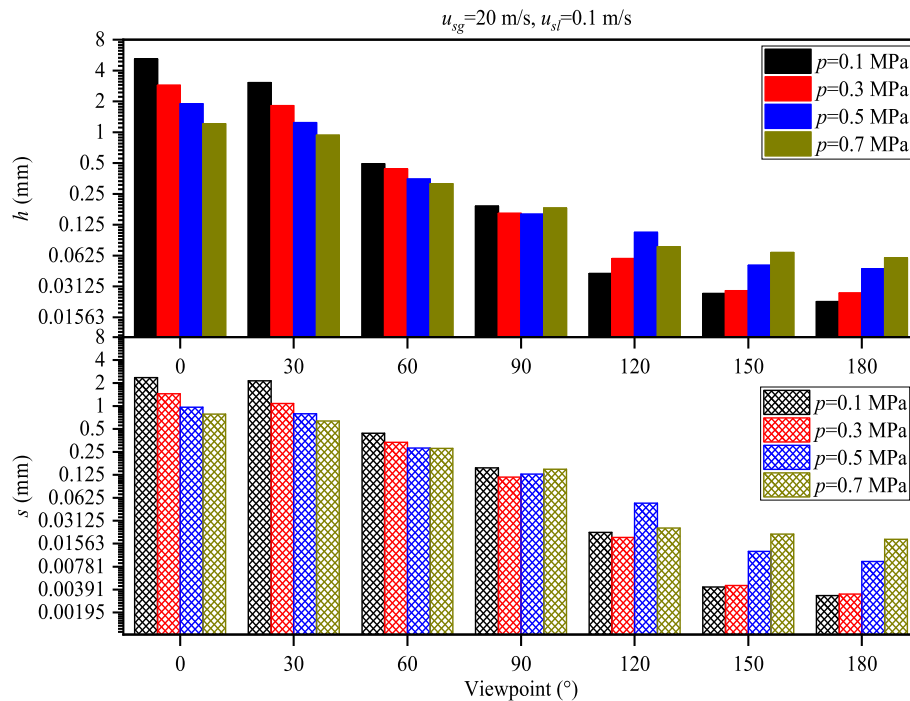


Fig. 9. The variation of liquid film with gas superficial velocity at different circumferential positions.



**Fig. 10.** The variation of liquid film with the apparent velocity of liquid phase at different circumferential positions.



**Fig. 11.** The variation of liquid film with system pressure at different circumferential positions.

where  $Re$  is the Reynolds number,  $\rho$  is the density,  $D$  is the inner diameter of the pipe,  $\mu$  is the dynamic viscosity, and the subscripts  $g$  and  $l$  represent gas phase and liquid phase, respectively.

In 1977, Tatterson et al. [18] pointed out that Henstock correlation does not consider the influence of gravity in vertical downflows at relatively low velocities. Therefore, based on Henstock correlation, the influence of gravity on the liquid film thickness was introduced, and a modified parameter  $F$  was proposed as shown in Eq. (8).

$$F = \frac{\gamma(Re_{lf})}{Re_g^{0.9}} \frac{\mu_l}{\mu_g} \frac{\rho_g^{0.5}}{\rho_l^{0.5}} \quad (8)$$

In 1998, a correlation to estimate the liquid film thickness of vertical upward annular flow was proposed by Fukano et al. [19], as shown in Eq. (9). The inner diameter of the experimental pipeline was 26 mm and the system pressure was 0.103–0.117 MPa.

**Table 2**  
Asymmetry of circumferential liquid film.

No.	$p$ (MPa)	$u_{sg}$ (m/s)	$u_{sl}$ (m/s)	$\bar{h}/h_0$	$h_{180}/h_0$
1	0.3	25	0.035	0.297	0.036
2			0.06	0.262	0.030
3			0.1	0.254	0.022
4		30	0.035	0.352	0.082
5			0.06	0.314	0.069
6			0.1	0.298	0.051
7	0.7	25	0.035	0.492	0.159
8			0.06	0.438	0.131
9			0.1	0.395	0.101
10		30	0.035	0.638	0.318
11			0.06	0.577	0.265
12			0.1	0.504	0.194

$$\frac{h}{D} = 0.0594 \exp\left(-0.34 Fr_g^{0.25} Re_l^{0.19} x^{0.6}\right) \quad (9)$$

$$x = \frac{u_{sg}\rho_g}{u_{sg}\rho_g + u_{sl}\rho_l} \quad (10)$$

where  $Fr$  is the Froude number,  $u$  is the superficial velocity, and  $x$  is the quality.

In 2009, Schubring et al. [20] used the iterative critical friction factor model to fit the liquid film thickness correlation by bringing a large number of experimental data of circumferential liquid film thickness of small diameter as shown in Eq. (11).

$$\frac{h}{D} = 4.7 \frac{1}{x} Re_G^{-\frac{2}{3}} \left(\frac{\rho_g}{\rho_l}\right)^{\frac{1}{3}} \quad (11)$$

$$Re_G = \frac{GD}{\mu_l} \quad (12)$$

where  $G$  is the mass flux.

In 2014, Berna et al. [21] analyzed the applicability of existing prediction correlations and proposed a comprehensive correlation based on a large number of experimental data under different working conditions as shown in Eq. (12).

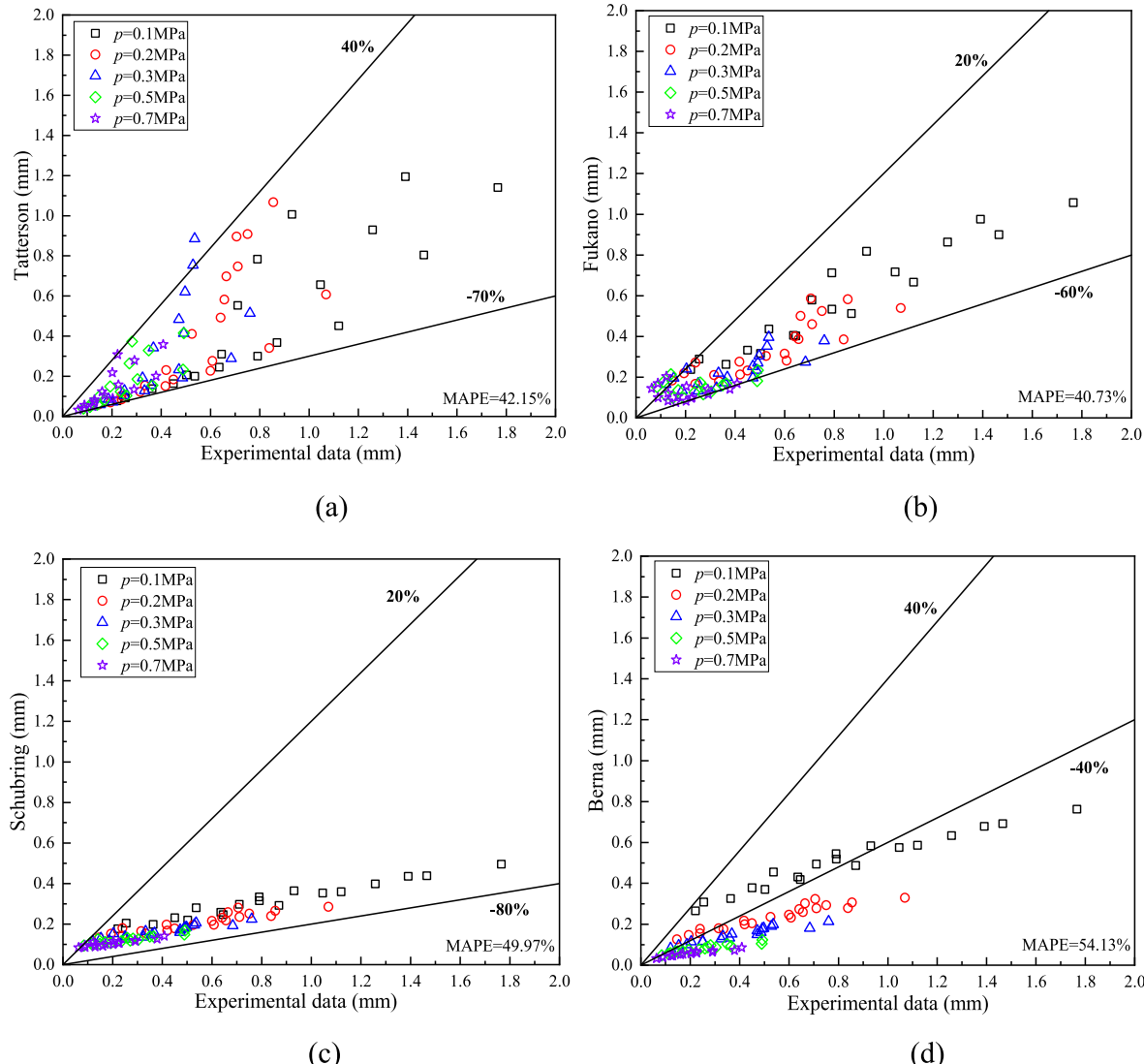


**Fig. 12.** Comparison of liquid film thickness between correlations with experiments.

$$h = 7.165 \text{Re}_g^{-1.07} \text{Re}_l^{0.48} \left( \frac{\text{Fr}_g}{\text{Fr}_l} \right)^{0.24} \quad (13)$$

In this paper, the errors of film thickness are evaluated by the relative error  $\epsilon$  and mean absolute percentage error MAPE between the experiments  $x_{exp}$  and correlations  $x_{corr}$  as follows.

$$\epsilon = \frac{x_{corr} - x_{exp}}{x_{exp}} \times 100\% \quad (14)$$

$$MAPE = \frac{1}{N} \sum_{i=1}^N \left| \frac{x_{corr,i} - x_{exp,i}}{x_{exp,i}} \right| \times 100\% \quad (15)$$

where  $N$  is the number of working conditions,  $i$  is the  $i$ -th working condition.

The working conditions are substituted into the four liquid film thickness correlations for prediction, and the predicted results are compared with the experimental measured values, as shown in Fig. 12.

Fig. 12(a) shows the comparison between the experimental data and the Tatterson correlation improved based on the Henstock correlation. Although the predicted results of this correlation are relatively scattered and the law is not obvious, the MAPE value is comparatively low, and the prediction performance is relatively good at high gas-liquid superficial velocity. The reason may be that the correlation considers the entrainment factor and the influence of gravity. However, its predictive performance for thicker liquid films is not ideal. This may be due to the lack of a large amount of horizontal experimental data during fitting.

In addition, the Fukano correlation compared with the experimental results is not ideal as shown in Fig. 12(b), especially for low gas velocity and high pressure conditions, where there is a significant deviation in the prediction of liquid film thickness. Fukano correlation is proposed based on the experimental data of vertical upward annular flow in the 26 mm pipe, and does not consider the influence of pressure on the liquid film thickness. Therefore, the predictive performance of liquid film thickness under different pipe diameters and different pressure is poor. However, it is worth affirming that Fukano correlation includes the influence factor of different liquid phase on the liquid film, which minimizes the overall error of the correlation.

Fig. 12(c) and (d) show that the correlations of Berna and Schubring are compared with the experiment. Both them show good regularity, especially the prediction values of Schubring correlation are more concentrated. This is because the Schubring correlation takes into account the influence of multiple pipe diameters when fitting. However, the selected pipe diameters are small, the prediction of the correlation has a certain deviation for other large pipe diameters. When the liquid film is thick, the predicted value is obviously smaller. The Berna correlation combines the well-behaved correlations in the existing literature, and considers a large number of experimental parameters, such as the gas and liquid superficial velocity, density, surface tension of liquid and dynamic viscosity of two fluids. Therefore, the regularity of the correlation is good, and the predicted values under normal pressure are more accurate than other correlations. Nevertheless, the Berna and Schubring correlations are not ideal for the liquid film thickness at medium and high pressures. Compared with the experimental, the liquid film thickness is underestimated.

Through the above analysis of the experimental data of liquid film thickness, there are two main problems at present. On the one hand, under the condition of high pressure, the predictive performance of the existing correlations are poor, which is due to the limitation of experimental conditions and the different explanations of the liquid film thickness theories by different scholars. On the other hand, the existing liquid film thickness correlations are mainly based on the prediction of a single pipe diameter, and there are few studies on prediction correlations of different pipe diameters. Therefore, the existing correlations cannot accurately predict the liquid film thickness under different working conditions. In order to solve the above problems, based on

Berna liquid film thickness prediction correlation, this paper fully integrates the advantages of the correlation described above, and a new liquid film thickness prediction correlation is established by introducing factors such as pressure, pipe diameter and droplet entrainment.

#### 4.2. New correlation of liquid film thickness

From the comparison results of the above correlations, it can be seen that the Berna and Schubring correlations are in good agreement with the experimental values, so this paper combines the advantages of the two correlations. Using the fitting parameters in the Berna correlation as the basis, referring Schubring correlation to the research ideas of fitting different pipe diameters and the improvement of Tatterson entrainment, a new liquid film thickness prediction correlation is established, as shown in Eq. (16).

$$h^* = a \left( \frac{D}{D_{ref}} \right)^b \text{Re}_g^c \text{Re}_{lf}^d \left( \frac{u_g}{u_l} \right)^e \left( \frac{p}{p_{ref}} \right)^f \quad (16)$$

where  $a, b, c, d, e, f$  are the fitting coefficients,  $\text{Re}_{lf}$  is the liquid film Reynolds number,  $D_{ref}$  is the reference diameter equal to 0.05 m,  $p_{ref}$  is the reference pressure equal to 0.1 MPa, and  $h^*$  is the dimensionless form of  $h$ . In 2000, Hurlburt [23] gave the specific relationship between  $h^*$  and  $h$ , as shown in Eq. (17).

$$h^* = \frac{h}{v_l \left( \rho_l \right)^{0.5}} \quad (17)$$

$$\tau_g = 0.023 \text{Re}_g^{-0.2} \rho_g u_{sg}^2 \quad (18)$$

where  $\tau_g$  is the gas phase shear force, and  $v_l$  is the liquid kinematical viscosity. For the liquid film Reynolds number  $\text{Re}_{lf}$ , its definition is as follows:

$$\text{Re}_{lf} = \frac{4m_l(1-E)}{\pi D \mu_l} = \text{Re}_l(1-E) \quad (19)$$

where  $m_l$  is the liquid mass flow rate and  $E$  is the entrainment rate.

Good predictive performance of improved droplet entrainment based on Tatterson correlation, this paper selects the correlation proposed by Lei Pan et al. [24] to solve the droplet entrainment rate and improve Berna correlation.

$$\frac{E/E_m}{1 - E/E_m} = B \left( \frac{D u_{sg}^3 \rho_l^{0.5} \rho_g^{0.5}}{\sigma} \right) \left( \frac{\rho_g^{1-m} \mu_g^m}{d_{32}^{1+m} g \rho_l} \right)^{1/(2-m)} \quad (20)$$

where  $A_2 = 9 \times 10^{-8}$ ,  $m = 0.6$ ,  $\sigma$  is the liquid surface tension, and the surface tension of water at 25 °C is 0.0718 N/m. Therefore, the average diameter of Sauter is  $d_{32}$  and the maximum entrainment rate is  $E_m$ , which can be obtained by the following correlation:

$$\frac{\rho_g u_{sg}^2 d_{32}}{\sigma} \left( \frac{d_{32}}{D} \right) = 0.0091 \quad (21)$$

$$E_m = 1 - \frac{m_{lfc}}{m_l} \quad (22)$$

$m_{lfc}$  is the critical liquid film mass flow rate, which can be calculated according to the following correlation.

$$m_{lfc} = 0.25 \cdot \mu_l \pi D \text{Re}_{lf} \quad (23)$$

$$\text{Re}_{lf} = 7.3(\log w)^3 + 44.2(\log w)^2 - 263 \log w + 439 \quad (24)$$

$$w = \frac{\mu_l}{\mu_g} \sqrt{\frac{\rho_g}{\rho_l}} \quad (25)$$

In order to obtain the fitting coefficient in Eq. (16), the nonlinear

least squares Levenberg-Marquardt iterative algorithm (LM algorithm) is used to fit the correlation of liquid film thickness prediction. Experimental data of  $p = 0.3, 0.5$  and  $0.7$  MPa, and all liquid film thickness data from Fukano and Luninski are selected, which include different pressures and different pipe diameters, and LM optimization iterative algorithm is used to bring the selected data into the correlation for training and optimization. A new relationship of liquid film thickness is obtained by  $a = 0.0207$ ,  $b = 0.6734$ ,  $c = -1.4343$ ,  $d = 1.8417$ ,  $e = 1.4062$ ,  $f = 1.2631$ . The fitting results are shown in Fig. 13. Comparing the selected fitting data with the new prediction model, it can be seen that the MAPE between the two is 8.82 %, and the relative error  $\varepsilon$  of more than 94 % of the liquid film thickness prediction results is within  $\pm 18\%$ , and the fitting effect is relatively good.

In order to further verify the extrapolation of the new correlation, the new correlation is compared with the existing liquid film thickness data, and the comparison results are shown in Fig. 14. It can be seen from the diagram that the MAPE of the new liquid film thickness prediction correlation is 11.08 %, and the relative error  $\varepsilon$  of 95 % of the liquid film thickness prediction results is within  $\pm 25\%$ . The prediction error is significantly reduced compared with the previous correlation, indicating that the new liquid film thickness prediction correlation has better extrapolation. In summary, the new liquid film thickness prediction correlation proposed in this paper not only considers the characteristics of pipeline diameter, pipeline pressure and droplet entrainment, but also has a good predictive performance on the liquid film thickness. The new model has a wide range of applicability.

## 5. Conclusion

In this paper, based on ultrasonic technology, the circumferential liquid film thickness under different pressures is obtained by simulation and experimental methods. Additionally, the liquid film thickness data under different pipe diameters are introduced, and the circumferential liquid film correlation suitable for different pressures and different pipe diameters is established. The main results are summarized as follows:

- (1) The measurement range of the UERMF method and the URSE method is compared by numerical simulation, and the minimum measurement range of these methods are 0.3 mm and 0.01 mm, respectively. Therefore, the URSE method is selected as the measurement method of this experiment.
- (2) The liquid film thickness under five system pressures from 0.1 MPa to 0.7 MPa is measured by the self-developed ultrasonic measurement system, and the fluctuation characteristics of liquid

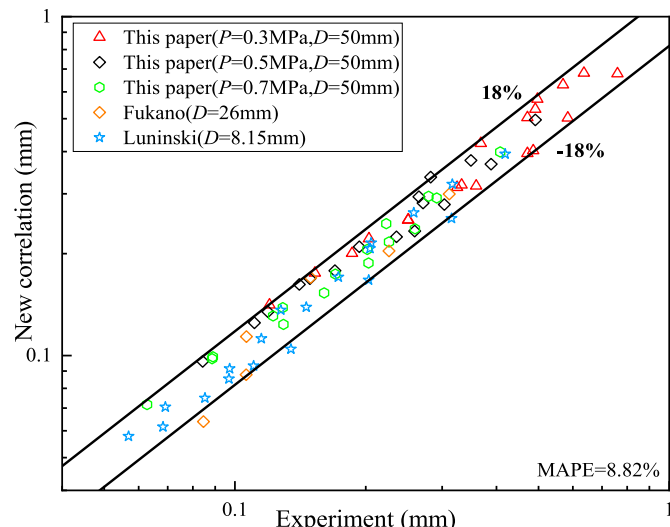


Fig. 13. The fitting results of partial data.

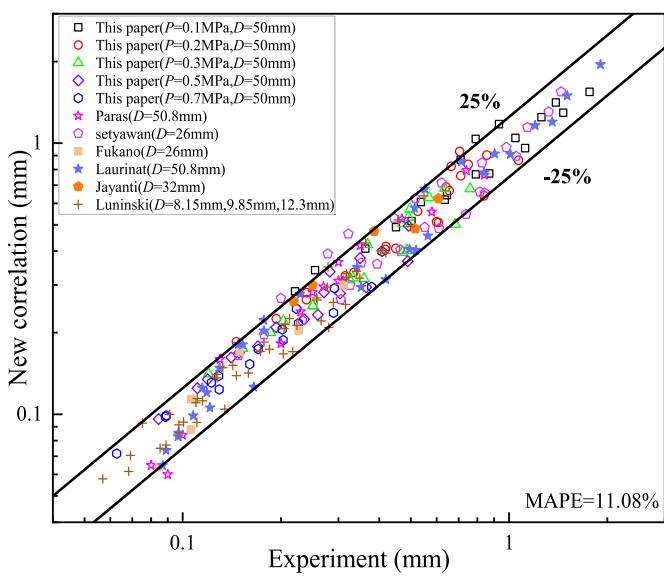


Fig. 14. Applicability of the new model.

film at different circumferential positions are analyzed. With the increase of  $u_{sg}$ , the lower liquid film becomes thinner and more stable, while the liquid film in the upper half of the pipeline shows an opposite changing trend, which reduces the asymmetry of the liquid film. With the increase of  $u_{sl}$ , the liquid film at each circumferential position shows an increasing trend, and the fluctuation of liquid film is more severe, also the asymmetry of circumferential liquid film is more serious. As the pressure increases, the liquid film in the lower half of the pipe decreases and becomes more stable, the upper liquid film becomes thicker and the fluctuation is more obvious, so the asymmetry of circumferential liquid film is weakened.

- (3) Due to the limited factors considered in existing correlations, accurately predicting the liquid film thickness at different pressures and pipe diameters becomes challenging. Therefore, the Berna correlation is optimized in this paper, factors such as pressure, pipe diameter and entrainment are introduced, and experimental data of different working conditions are substituted into the correlation for parameter fitting. In order to verify the applicability of the correlation, the existing data are substituted into the new correlation. The relative errors of more than 95 % of the experimental data are within  $\pm 25\%$ , and the MAPE is 11.08 %, indicating that the introduced parameters can fully reflect the influence of system pressure and pipe diameter on liquid film thickness. The improved correlation is applicable to horizontal annular flow and high pressure systems. Thus, the extrapolation and applicability of the new liquid film thickness correlation are verified.

## CRediT authorship contribution statement

**Mi Wang:** Conceptualization, Data curation, Funding acquisition, Investigation, Methodology, Writing - original draft, Writing - review & editing. **Yuxin Bai:** Data curation, Investigation, Software, Validation, Writing - original draft, Writing - review & editing. **Jiegui Liu:** Data curation, Investigation, Software, Validation. **Dandan Zheng:** Conceptualization, Funding acquisition, Project administration, Resources. **Lide Fang:** Funding acquisition, Project administration, Resources.

## Declaration of competing interest

The authors declare that they have no known competing financial

interests or personal relationships that could have appeared to influence the work reported in this paper.

## Data availability

The authors are unable or have chosen not to specify which data has been used.

## Acknowledgements

This work is supported by the Advanced Talents Incubation Program of Hebei University (No. 521100222043) and the National Natural Science Foundation of China (No. 62071321, 62173122).

## References

- [1] M. Faroughi, M. Karimimoshaver, F. Aram, E. Solgi, A. Mosavi, N. Nabipour, K.-W. Chau, Computational modeling of land surface temperature using remote sensing data to investigate the spatial arrangement of buildings and energy consumption relationship, *Eng. Appl. Comput. Fluid Mech.* 14 (1) (2020) 254–270, <https://doi.org/10.1080/19942060.2019.1707711>.
- [2] Y. Xu, C. Yuan, Z. Long, Q. Zhang, Z. Li, T. Zhang, Research the wet gas flow measurement based on dual-throttle device, *Flow Meas. Instrum.* 34 (2013) 68–75, <https://doi.org/10.1016/j.flowmeasinst.2013.07.014>.
- [3] Q. Chen, T. Xiong, X. Zhang, P. Jiang, Study of the hydraulic transport of non-spherical particles in a pipeline based on the CFD-dem, *Eng. Appl. Comput. Fluid Mech.* 14 (1) (2019) 53–69, <https://doi.org/10.1080/19942060.2019.1683075>.
- [4] A. Cioncolini, J.R. Thome, Liquid film circumferential asymmetry prediction in horizontal annular two-phase flow, *Int. J. Multiphas. Flow* 51 (2013) 44–54, <https://doi.org/10.1016/j.ijmultiphaseflow.2012.12.003>.
- [5] T. Takamasa, K. Kobayashi, Measuring interfacial waves on film flowing down tube inner wall using laser focus displacement meter, *Int. J. Multiphas. Flow* 26 (9) (2000) 1493–1507, [https://doi.org/10.1016/s0301-9322\(99\)00099-3](https://doi.org/10.1016/s0301-9322(99)00099-3).
- [6] L. Zhai, H. Zhang, C. Yan, N. Jin, Measurement of oil–water interface characteristics in horizontal pipe using a conductance parallel-wire array probe, *IEEE Trans. Instrum. Meas.* 68 (9) (2019) 3232–3243, <https://doi.org/10.1109/tim.2018.2877221>.
- [7] Y. Zhao, Q.C. Bi, H.C. Lv, R.C. Hu, Study of the characteristics of an annular flow liquid film and disturbance waves in a vertical riser by using gamma rays, *J. Eng. Therm. Energy Power* 29 (2014) 53–57. <https://doi.org/10.16146/j.cnki.rndlgc.2014.01.01>.
- [8] Z. Deng, Z. Huang, Y. Shen, Y. Huang, H. Ding, A. Luscombe, M. Johnson, J. E. Harlow, R. Gauthier, J.R. Dahn, Ultrasonic scanning to observe wetting and “unwetting” in li-ion pouch cells, *Joule* 4 (9) (2020) 2017–2029, <https://doi.org/10.1016/j.joule.2020.07.014>.
- [9] J. Park, M.H. Chun, S.K. Lee, Liquid film thickness measurement by an ultrasonic pulse echo method, *Nucl. Eng. Technol.* 17 (1985) 25–33.
- [10] W. Ren, N. Jin, L. Zhai, Y. Ren, Measurement of liquid film thickness in vertical multiphase slug and churn flows using distributed ultrasonic method, *IEEE Sensor.* J. 19 (22) (2019) 10537–10544, <https://doi.org/10.1109/jsen.2019.2931190>.
- [11] R.S. Dwyer-Joyce, B.W. Drinkwater, C.J. Donohoe, The measurement of lubricant–film thickness using ultrasound, *Proc. Royal Soc. Lond. Series A: Math. Phys. Eng. Sci.* 459 (2032) (2003) 957–976, <https://doi.org/10.1098/rspa.2002.1018>.
- [12] R.S. Dwyer-Joyce, P. Harper, B.W. Drinkwater, A method for the measurement of hydrodynamic oil films using ultrasonic reflection, *Tribol. Lett.* 17 (2) (2004) 337–348, <https://doi.org/10.1023/b:tril.0000032472.64419.1f>.
- [13] M. Wang, D. Zheng, Y. Xu, A new method for liquid film thickness measurement based on ultrasonic echo resonance technique in gas–liquid flow, *Measurement* 146 (2019) 447–457, <https://doi.org/10.1016/j.measurement.2019.06.027>.
- [14] G. Aoyama, T. Nagayoshi, A. Baba, Preliminary test of an ultrasonic liquid film sensor for high-temperature steam–water two-phase flow experiments, *J. Nucl. Sci. Technol.* 51 (3) (2014) 350–358, <https://doi.org/10.1080/00223131.2013.871589>.
- [15] B. Praher, G. Steinbichler, Ultrasound-based measurement of liquid-layer thickness: a novel time-domain approach, *Mech. Syst. Signal Process.* 82 (2017) 166–177, <https://doi.org/10.1016/j.ymssp.2016.05.016>.
- [16] Y.A. Al-Aufi, B.N. Hewakandamby, G. Dimitrakis, M. Holmes, A. Hasan, N. J. Watson, Thin film thickness measurements in two phase annular flows using ultrasonic pulse echo techniques, *Flow Meas. Instrum.* 66 (2019) 67–78, <https://doi.org/10.1016/j.flowmeasinst.2019.02.008>.
- [17] W.H. Henstock, T.J. Hanratty, The interfacial drag and the height of the wall layer in annular flows, *AICHE J.* 22 (6) (1976) 990–1000, <https://doi.org/10.1002/aic.690220607>.
- [18] D.F. Tatterson, J.C. Dallman, T.J. Hanratty, Drop sizes in annular gas–liquid flows, *AICHE J.* 23 (1) (1977) 68–76, <https://doi.org/10.1002/aic.690230112>.
- [19] T. Fukano, T. Furukawa, Prediction of the effects of liquid viscosity on interfacial shear stress and frictional pressure drop in vertical upward gas–liquid annular flow, *Int. J. Multiphas. Flow* 24 (4) (1998) 587–603, [https://doi.org/10.1016/s0301-9322\(97\)00070-0](https://doi.org/10.1016/s0301-9322(97)00070-0).
- [20] D. Schubring, T.A. Shedd, Critical friction factor modeling of horizontal annular base film thickness, *Int. J. Multiphas. Flow* 35 (4) (2009) 389–397, <https://doi.org/10.1016/j.ijmultiphaseflow.2008.12.002>.
- [21] C. Berna, A. Escrivá, J.L. Muñoz-Cobo, L.E. Herranz, Review of droplet entrainment in annular flow: interfacial waves and onset of entrainment, *Prog. Nucl. Energy* 74 (2014) 14–43, <https://doi.org/10.1016/j.pnucene.2014.01.018>.
- [22] A. Setyawan, Indarto, Deendarlianto, Experimental investigations of the circumferential liquid film distribution of air–water annular two-phase flow in a horizontal pipe, *Exp. Therm. Fluid Sci.* 85 (2017) 95–118, <https://doi.org/10.1016/j.expthermflusci.2017.02.026>.
- [23] E.T. Hurlbut, T.A. Newell, Prediction of the circumferential film thickness distribution in horizontal annular gas–liquid flow, *J. Fluid Eng.* 122 (2) (2000) 396–402, <https://doi.org/10.1115/1.483269>.
- [24] L. Pan, T.J. Hanratty, Correlation of entrainment for annular flow in horizontal pipes, *Int. J. Multiphas. Flow* 28 (3) (2002) 385–408, [https://doi.org/10.1016/s0301-9322\(01\)00074-x](https://doi.org/10.1016/s0301-9322(01)00074-x).
- [25] M. Wang, D. Zheng, W. Wang, Measurement of circumferential liquid film thickness in horizontal gas–liquid annular flow using ultrasound, in: 2021 IEEE International Instrumentation and Measurement Technology Conference (I2MTC), 2021, pp. 1–6, <https://doi.org/10.1109/I2MTC50364.2021.9459849>.